Build Simul (2015) 8: 81 – 98
DOI 10.1007/s12273-014-0195-2

Outdoor ventilation performance of various configurations of a layout of two adjacent buildings under isothermal conditions

Samuel Adinoyi Ayo[1,2] (✉), Normah Mohd-Ghazali[1], Shuhaimi Mansor[1]

1. Faculty of Mechanical Engineering, Universiti Teknologi Malaysia, 81310 Johor Bahru, Johor, Malaysia
2. Department of Mechanical Engineering, Federal University of Technology Minna, Nigeria

Abstract

This paper explores the pedestrian-level wind environment around two buildings of unequal heights for the effects of ratio of height of upwind building to that of downwind building, referred to as buildings height ratio, spacing distance between the buildings, and direction of ambient wind, on the outdoor air ventilation. The objective is to propose appropriate spacing distances for various configurations of this type of buildings layout in a suburban area of Kuala Lumpur, which would enable harnessing the full ventilation potential of the local wind conditions. A three-dimensional numerical technique employing computational fluid dynamics simulation of continuity and Reynolds-Averaged Navier–Stokes equations was used to study the turbulent flow field around the full-scale sizes of the buildings. Results indicate the influence of spacing distance between buildings, relative heights of the buildings and direction of ambient wind on outdoor ventilation. Results also show that 3-D turbulent flow processes such as lateral and secondary flows play significant roles in defining the wind flow pattern and ventilation availability. The perpendicular wind direction presents remarkable adverse effects compared to the inclined direction, while a higher upwind building height which would ordinarily be expected to proportionally obstruct wind flow could be of advantage, at low values of building height ratios, in enhancing outdoor ventilation. The findings established the need to give consideration to climatic factors such as wind flow and direction in planning urban cities, as it affects buildings to be situated in close proximity, especially when there is height difference.

Keywords

outdoor air ventilation,
computational fluid dynamics,
appropriate spacing distance,
height ratio,
wind direction,
two-building layout

Article History

Received: 20 January 2014
Revised: 30 July 2014
Accepted: 4 August 2014

1 Introduction

In an urban area, the main characteristic features which directly impact on human thermal comfort and environmental health are the high volume of vehicular traffic and building density. The high volume of street vehicles has been identified as the major source of pollutants in the urban outdoor environment (Fenger 1999; Li et al. 2006; Xie et al. 2006a; Popescu 2011), while the buildings, which usually include many medium- and high-rise buildings, act as obstacles to the free flow of air and dispersion of pollutants (Cheng et al. 2008; Yim et al. 2009; Cheung and Liu 2011). This usually results in low urban wind speeds, poor street ventilation and accumulation of pollutants, especially at the pedestrian level, and particularly in low wind cities. The ambient temperature may also rise. The building indoor environment is similarly affected as the conditions depend on those of the outdoor climate (Givoni 1998; Allard and Ghiaus 2005; Ji and Zhao 2014). The low air quality and air movement have direct adverse impacts on the environmental health of the occupants and their physiological perception of the thermal environment (Bottema 1993). Besides factors due to meteorological conditions such as wind speed and direction, and level of turbulence, wind flow and pollutant dispersion from a street canyon depend on street dimensions and building geometry and layout (Li et al. 2006; Xie et al. 2006b). But despite the numerous research works on outdoor ventilation, literature is scarce on studies focused on prescribing appropriate spacing distances between buildings for maximum outdoor ventilation from ambient wind that

E-mail: sa_ayo@yahoo.com

List of symbols

AER	dimensionless air exchange rate	$\overline{U}_i$	mean velocity vectors in the x-, y- and z-directions (m/s); $\overline{U}_i = (\overline{u}, \overline{v}, \overline{w})$
H	height of downwind building (m)		
HR	height ratio	u''_i	velocity fluctuation vectors in the x-, y- and z-directions (m/s); $u''_i = (u'', v'', w'')$
$\overline{P}$	mean pressure (kg/(m·s^2))		
Re_H	Reynolds number based on height H of downwind building	VR	velocity ratio
		x_i	three components (x, y, z) of space coordinates in the stream-wise, vertical, and lateral directions (m)
S	spacing distance (m)		
t	time (s)	ρ	density of air (kg/m^3)

consider three-dimensional effects of turbulent flow and using representative scales of actual building.

Research works on the wind field and flow structure around buildings and over an urban area and the effects of ambient wind conditions, building geometry and street dimensions date back several years ago. Most of the early works conducted in these areas were by field measurements and/or physical modelling (Ogawa and Oikawa 1982; DePaul and Sheih 1985; Maruyama and Ishizaki 1988; Oke 1988; Li et al. 1998; Baik et al. 2000; Uehara et al. 2000; Kastner-Klein et al. 2001), while a few others were by numerical modelling (Sini et al. 1996; Baik and Kim 1999; Kim and Baik 1999). The studies were used, essentially, to identify the different flow regimes, and the patterns and structures of the flow. Subsequent studies (Xie et al. 2003; Xie et al. 2005, 2006a; Allard and Ghiaus 2005; Li et al. 2006; Wang and Huang 2006; Wang et al. 2006; Li et al. 2009; Gao et al. 2012) were used to study these flow characteristics in greater details. Some of these latter studies investigated the blockage effects involving buildings in close proximity to wind flow around the buildings (Xie et al. 2005, 2006a;Wang and Huang 2006; Wang et al. 2006). Xie et al. (2005) in a two-dimensional (2-D) numerical simulation, examined the impact of ambient buildings on the quality of air in street canyons. They used four different configurations of linear arrays for each of four buildings, and reported that pollutant concentration was higher in the canyon when the windward building of the downwind street was vertically enhanced and when there was no enhancement at all, compared to when the extreme right building in the array was enhanced and when both the extreme right and left buildings in the array were enhanced. The study highlights not only the importance of street canyon buildings, but also that of ambient buildings. Wang and Huang (2006) conducted a 2-D numerical study of wind flow and pollutant dispersion in asymmetrical urban street canyon. They used various configurations of a two-building layout with heights of the upwind and downwind buildings as variables and observed that the asymmetrical configurations have obvious impacts on the airflow structure and dispersion pattern, different from that of the symmetrical configuration. They also observed increase in total concentration with increase in height of upwind or downwind building up to the point when the difference in height was about 5 m and reported lower total pollutant concentration in the step-down configuration (higher upwind building) than in the step-up configuration (higher downwind building) and the symmetrical configuration of reverse height ratio. In a related study, Wang et al. (2006) sought to optimize urban street canyon layout for best design from the viewpoint of environmental protection using 2-D numerical simulation coupled with mathematical optimization. They followed a procedure similar to that of Wang and Huang (2006) and obtained the optimized configuration, which favoured lowest pollutant (carbon monoxide, CO) concentration accumulation within the canyon, to be the step-down configuration with a proper height difference. The total concentration in the symmetrical type of canyon was also determined to be highest. In a more comprehensive study, Xie et al. (2006a) conducted a 2-D numerical simulation to examine the impact of street geometry on the local atmospheric environment. Various configurations of the street geometry were formed by varying the heights of the upwind and downwind buildings, as well as the street width. They reported that pollutant concentration was the highest in the narrow-street multi-vortex regime due to the weak vortex formed at the street level and the highly reduced mean horizontal wind speed, all of which resulted in a sheltering effect at the pedestrian level. They also reported lowest concentration in the wider canyon regime with fewer vortices. From the foregoing literature, it would be noted that most of the studies were based on two-dimensional configurations of the physical model. These are highly simplified configurations of the real system and represent street canyons with infinite length in the spanwise direction. One of the limitations of this simplification is that it neglects the effects of the double-eddy recirculation that form at the leeward side of a

building. This and the 3-D lateral and secondary flows which strongly influence the vertical mixing of pollutants concentration and the distribution of the pollutants around the building are observed only in 3-D situations (Li et al. 2006; Heist et al. 2009; Brixey et al. 2009). Obviously 2-D simulations neglect these effects, and any findings that would represent the real situation should reflect the effects of these turbulent flow processes. In actual urban settings with limited canyon axial geometry, three-dimensional effects such as end flows and lateral flows are present (Li et al. 2006; Heist et al. 2009; Brixey et al. 2009) and are expected to play significant roles in defining the flow structure, wind flow pattern and the air ventilation availability within the street, especially at the pedestrian level. In addition to the observed limitations of the 2-D studies, the wind velocities used in the studies have also been arbitrarily chosen, and not with reference to the meteorological data of a real urban city. Besides, the works have not been used to fully explore the ventilation effect of high-rise buildings in the neighbourhood of low-rise buildings with a view to prescribing appropriate spacing distances between the buildings, for various configurations, for the purpose of adequate air ventilation.

More recent studies on the effects of adjacent or ambient buildings on outdoor air ventilation in a street canyon either adopted the 3-D numerical simulation approach in order to make the findings more realistic, make use of knowledge of site wind environmental conditions, or are based on field measurement (Yim et al. 2009; Heist et al. 2009; Brixey et al. 2009; Bourbia and Boucheriba 2010; Buccolieri et al. 2010; Cheung and Liu 2011; Krüger et al. 2011; Gu et al. 2011; Hang et al. 2012; Panagiotou et al. 2013; Yuan et al. 2014). A typical coastal urban setting in Hong Kong consisting of some blocks of high-rise buildings and low-rise buildings was chosen by Yim et al. (2009) to investigate the impact of the upwind location of the high-rise buildings on the air ventilation and pollution dispersion in the street canyons of the low-rise buildings. They considered the height of the high-rise buildings and the direction of wind as variables, while the buildings separation and height of low-rise buildings were held constant. They reported reduction in the outdoor air ventilation around the low-rise building array with increase in height of high-rise buildings. Heist et al. (2009) and Brixey et al. (2009) used both wind tunnel experiment and CFD numerical simulations to design a model to simulate an area of Brooklyn, New York, USA, to examine the effects of a tall tower on the flow characteristics and pollutant dispersion around a uniform array of buildings. They reported that the tall tower situated within the array of buildings caused increased velocities in the street canyons and enhanced exchange of flow between the canyons and the upper atmosphere, leading to better ventilation of the canyons and deceased residence time of pollutants in the wake of the tower. They attributed this to the occurrence of lateral flow perpendicular to the prevailing winds aloft, in addition to the downward and upward flow motions at the upwind and downwind sides of the tower, respectively, which was triggered by the presence of the tower. Bourbia and Boucheriba (2010) carried out a field experiment at several urban sites of the semi-arid Constantine City, Algeria to assess the impact of street canyon geometry on the street climate of the built environment. They utilized several sites of different geometric configurations of the urban streets and reported that a negative correlation of building height/street width ratio with air and surface temperatures. Airflow within the street was not measured. CFD numerical simulation was conducted by Buccolieri et al. (2010) to examine the influence of building packing density on flow and pollutant removal in order to assess the optimum neighbourhood building layout that minimizes pollution level. They reported that the ventilation of the canopy strongly depends on building packing density. They also observed airflow to enter the building array through the lateral side and exit through the street top when the packing density was significant. This highlights the importance of lateral flow on outdoor ventilation of urban neighbourhoods. Cheung and Liu (2011) conducted 3-D numerical simulation to study the effects of building interference on the ventilation of hypothetical apartments in a building cluster, using an average wind data for most urban regions in Hong Kong for a certain period of time. The study was focused on internal flow. However, it was revealed that blockages from the upwind buildings effected air ventilation into the buildings and that the level of blockages was affected by building separation and disposition. Krüger et al. (2011) used field experiment measurement to investigate the impact of urban geometry on the thermal comfort and air quality of the outdoor environment of a pedestrian street of a Brazilian city centre and reported that urban geometry has impact on human comfort. The airflow and pollutant dispersion characteristics of uneven building layout in non-homogeneous street canyons were investigated by Gu et al. (2011) and they reported that there were more complicated flow structures in non-uniform street canyons compared to those in uniform street canyons, which support large scale exchange of air masses between the canyon and the flow above. They suggested that uneven building layout could improve pollutant dispersion in an urban area. Hang et al. (2012) numerically investigated the vertical ventilation flow rate and pollutant removal mechanism in idealized urban-like geometries with different height variabilities and compared the results to those of arrays with uniform heights. They reported that arrays of height variabilities with large standard deviations tend to induce better pedestrian level ventilation. They also reported that arrays with very

large standard deviations tend to induce better pedestrian level ventilation through the horizontal mean flow and turbulent diffusivity vertical mean flow, compared to uniform arrays that would require modification to the street canyon geometry. Panagiotou et al. (2013) also used CFD simulations to study the city breathability of an inhomogeneous neighbourhood area of central London for the airflow and induced flow exchange processes in the area. They adopted the criterion of exchange velocity and reported that the exchange processes with the flow above, which depend on the shapes and sizes of the vertical structures, are determined by the building shapes and street canyon geometries and that the exchange velocity is higher in inhomogeneous urban neighbourhood than that in regular homogeneous setting. A CFD parametric study was conducted by Yuan et al. (2014) to examine the impact of urban permeability and building geometries on air pollution and noted that strategies which promote the dispersion of pollutants in high-density cities include building separation and porosity. It would be observed that the studies just reviewed did not examine the parametric impacts of building geometry together with the layout, particularly the building height and the spacing distance between the buildings on the outdoor ventilation. Such studies are needed in order to be able to develop practical air ventilation data applicable for use as part of the factors to be considered for developing more comprehensive guidelines for building layout for an urban area. The present study is aimed at achieving such objective for a low wind urban area with hot and humid climatic conditions, using the actual wind data and representative building dimensions for the area.

2 Methodology of the study

2.1 Urban area studied

The present work was used to simulate the interference effects of a high-rise building to wind flow around a lower-height building situated downwind for various street widths and heights of the high-rise building. This preliminary study uses two blocks of single-loaded closed-corridor apartment buildings models with the dimensions of the rectangular plan greater than the minimum specified in the Malaysia Uniform Building By-Laws 1984 (Ubbl 2006 Amendment) to represent the two-building structure. A ten-year wind data (2003–2012) obtained from the Malaysia (Subang) Meteorological Data was used to develop a wind profile for the area. The Peninsular Malaysia has a hot and humid tropical climate system (Zain et al. 2007), with a mild mean surface wind of about 1.5 m/s at the measurement station and a maximum of less than 8 m/s, but which is above the indoor air speed range of between 0.1 and 1.5 m/s needed for a satisfactory comfort conditions (Ismail 1996). With a compact urban setting, the street air ventilation can fall far below the required level and give rise to thermal comfort and environmental health issues for the occupants. However, with proper building design and layout on a case-by-case basis, this level of air movement can be harnessed, to provide a thermally comfortable environment reaching down to the pedestrian level.

2.2 Problem formulation and physical model

Wind flow in urban areas is an urban boundary layer flow, which has been generally recognised as a turbulent flow. This is confirmed for the case under study by the flow critical Reynolds number in Section 3.1. The flow is, therefore, described by the well-known basic equations of continuity and Navier–Stokes momentum equations. The solution method adopted is the CFD numerical technique based on the Reynolds Averaged Navier–Stokes (RANS) approach in which the instantaneous basic flow equations are averaged in time over all the turbulent scales. An isothermal case is considered, and the flow around the area modelled is assumed a constant density incompressible flow (Sini et al. 1996; Xie et al. 2005). The resulting statistically averaged 3-D continuity and RANS equations can be expressed, respectively, as follows:

$$\frac{\partial \overline{U}_i}{\partial x_i} = 0 \tag{1}$$

$$\overline{U}_j \frac{\partial \overline{U}_i}{\partial x_j} = -\frac{1}{\rho}\frac{\partial \overline{P}}{\partial x_i} + \frac{\partial}{\partial x_j}\left(\nu \frac{\partial \overline{U}_i}{\partial x_j} - \overline{u''_i u''_j}\right) \tag{2}$$

The model equations were closed by the realizable k–ε (RKE) turbulence model (Shih et al. 1995). The model has been used in previous studies and it was reported to perform quite well for the prediction of wind flow around buildings (Franke et al. 2004; Blocken et al. 2007; Yim et al. 2009; van Hooff and Blocken 2010). The transport equations for turbulent kinetic energy k and rate of dissipation of turbulent kinetic energy ε for the model can be expressed, respectively, as follows:

$$\overline{U}_i \frac{\partial k}{\partial x_i} = \frac{1}{\rho}\frac{\partial}{\partial x_i}\left\{\left(\mu + \frac{\mu_t}{\sigma_k}\right)\right\}\frac{\partial k}{\partial x_i} + \frac{1}{\rho}P_k - \varepsilon \tag{3}$$

$$\overline{U}_i \frac{\partial \varepsilon}{\partial x_i} = \frac{1}{\rho}\frac{\partial}{\partial x_i}\left\{\left(\mu + \frac{\mu_t}{\sigma_\varepsilon}\right)\right\}\frac{\partial \varepsilon}{\partial x_i} + C_1 S\varepsilon - C_2 \frac{\varepsilon^2}{k + \sqrt{\nu\varepsilon}} \tag{4}$$

where, $\overline{u''_i u''_j} = \frac{2}{3}k\delta_{ij} - \nu_t\left(\frac{\partial \overline{U}_i}{\partial x_j} + \frac{\partial \overline{U}_j}{\partial x_i}\right)$; $P_k = \nu_t\left(\frac{\partial \overline{U}_i}{\partial x_j} +$

$$\frac{\partial \overline{U}_j}{\partial x_i}\Big)\frac{\partial \overline{U}_i}{\partial x_j};\quad \nu_t=\frac{\mu_t}{\rho};\quad \mu_t=\rho C_\mu\frac{k^2}{\varepsilon};\quad C_\mu=\frac{1}{A_0+A_s\dfrac{kU^*}{\varepsilon}};$$

$$A_0=4.04\quad;\quad A_s=\sqrt{6}\cos\phi\quad;\quad \phi=\frac{1}{3}\cos^{-1}\left(\sqrt{6}W\right)\quad;$$

$$W=\frac{S_{ij}S_{jk}S_{ki}}{\tilde{S}^3};\quad S_{ij}=\frac{1}{2}\left\{\frac{\partial \overline{U}_j}{\partial x_i}+\frac{\partial \overline{U}_i}{\partial x_j}\right\};\quad U^*=\tilde{S}=\sqrt{S_{ij}S_{ij}};$$

$$C_1=\max\left[0.43,\frac{\eta}{\eta+5}\right];\quad \eta=S\frac{k}{\varepsilon};\quad S=\sqrt{2S_{ij}S_{ij}}.$$

$C_{1\varepsilon}, C_2, \sigma_k$, and σ_ε are model constants and have values as follows: $C_{1\varepsilon}=1.44$, $C_2=1.9$, $\sigma_k=1.0$, $\sigma_\varepsilon=1.2$.

The model equations were computed using the commercial CFD codes ANSYS Fluent 14.0 (ANSYS 2011).

2.3 Model validation

The CFD turbulence model was validated against results of wind tunnel experiment carried out by the Architectural Institute of Japan (AIJ) for the guideline on CFD prediction of pedestrian wind environment around buildings (Tominaga et al. 2004) to obtain the flow field around the model of a single high-rise building as a test case for the cross comparison of CFD results of various turbulence models. The geometry of the building model has scale ratio 4:4:1 (height: width: depth), with a depth of 0.05 m. The geometry is as shown in Fig. 1. The wind tunnel test section has dimensions 1.65 m × 1.6 m × 1.65 m (width × height × length). In the experiment, the mean wind velocity and the instantaneous components of velocities in the *x*-, *y*- and *z*-directions were measured using split fibre anemometer. Measurements were taken at 115 points in a horizontal plane at 12.5 mm height from the base floor and at 109 points in the vertical plane of symmetry. Figure 2 shows the locations of measurement of the wind profiles. The computational domain was designed according to the recommendations of major CFD guidelines and past studies (Franke et al. 2004; Franke 2006; Franke et al. 2007; Tominaga et al. 2008). The inflow boundary, and the lateral and top boundaries were set 5*h*

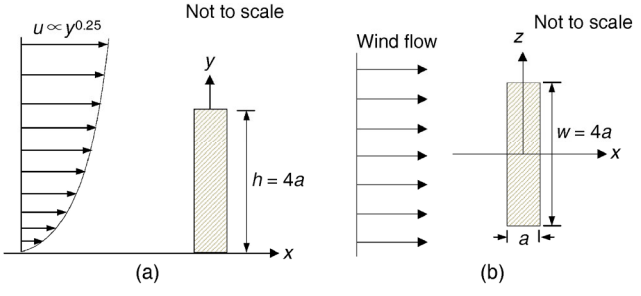

Fig. 1 Model with the approach wind speed profile: (a) side view; (b) top view

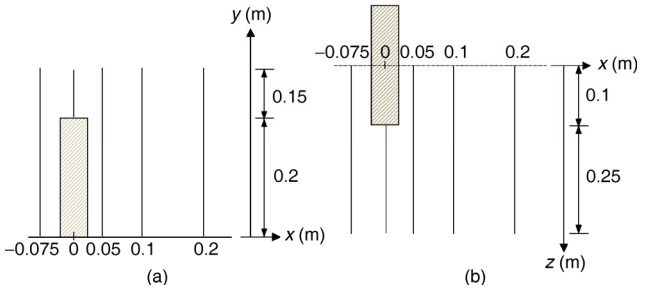

Fig. 2 Locations of measurement of wind profiles: (a) locations on the vertical plane along the centreline of the building; (b) locations on the horizontal plane at $y = 0.0125$ m $\left(\frac{1}{16}h\right)$. Direction of flow is from left to right

away from the building, where *h* is the height of the model building, while the outflow boundary was located 15*h* behind the building in order to allow for the flow to become fully redeveloped. The dimensions of the computational domain are as shown in Fig. 3. The domain was discretized using ANSY Meshing 14.0 (ANSYS 2011).

The measured inflow vertical velocity profile, which has a reference velocity of 7.84 m/s at 1.0 m height, closely follows the power law profile with exponent 0.25, while the data for the inflow turbulent kinetic energy and the rate of dissipation of turbulent kinetic energy were interpolated with closely approximating functions. The boundary conditions for the ground and building surfaces were specified by the wall-function based on the logarithmic law with roughness length parameter. The roughness length $y_0 = 9.6 \times 10^{-5}$ m was specified for the ground surface, while the smooth wall condition was prescribed on the building surfaces. The downstream boundary conditions were specified by zero normal gradients of all variables, while the lateral and upper surfaces were assigned the inviscid wall conditions by which the normal velocity components and normal gradient of tangential velocity components on the affected boundaries were set to zero.

The validation results of the CFD RKE turbulence model are as presented in Figs. 5–8. Figures 5(a)–(e) compare the simulation results of the mean streamwise wind velocity component at various locations on a vertical plane along the

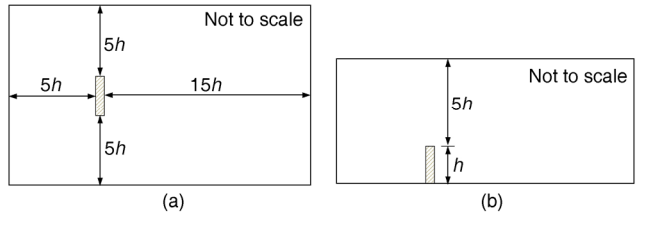

Fig. 3 Geometry of the computational domain of the CFD validation model: (a) side view; (b) top view

centreline of the building with the wind tunnel experimental data, while Figs. 6(a)–(e) compare the same velocity component at similar locations but on a horizontal plane at $y = 0.0125$ m (near the ground surface), for half domain. Figure 4 shows the lee eddy recirculations on the vertical plane along the centreline of the building and the transverse ground level double eddy recirculation behind the building. It was observed from Figs. 5(a)–(e) that the mean streamwise wind velocity agreed very well with the experimental data at the measuring points in front of and behind the building. The lee eddy recirculations behind the building were also reproduced by the calculations except that in the region close to the building surface, the point of transition of the average streamwise velocity from negative to positive values was calculated a little lower on the vertical axis. This may be due to the slight overestimation of the size of the recirculation behind the building usually associated with RANS models. This caused the centre of the vortex to be shifted further downwind. On the horizontal plane at $y = 0.0125$ m illustrated in Fig. 6, the model was able to capture the transverse ground level double eddy recirculation behind the building (see Fig. 4). However, the size of the recirculation eddy was predicted a little larger than in the experiment, probably for the same reason mentioned before.

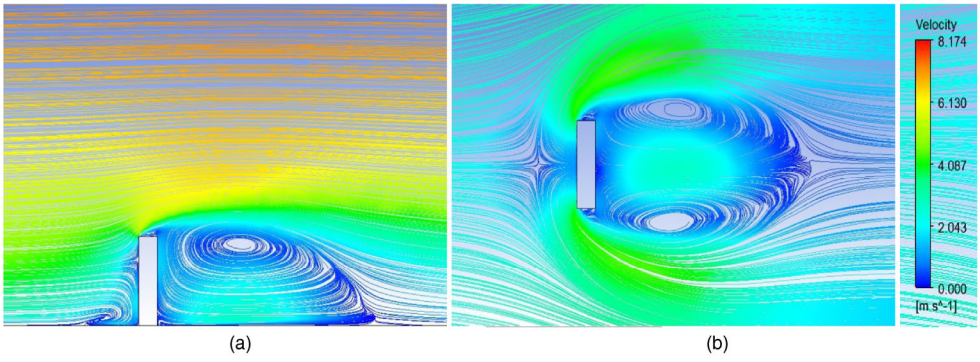

Fig. 4 Recirculating eddies of the validation building model: (a) lee eddy recirculations on the vertical plane along the centreline of the building; (b) transverse ground level double eddy recirculations behind the building. Direction of flow is from left to right

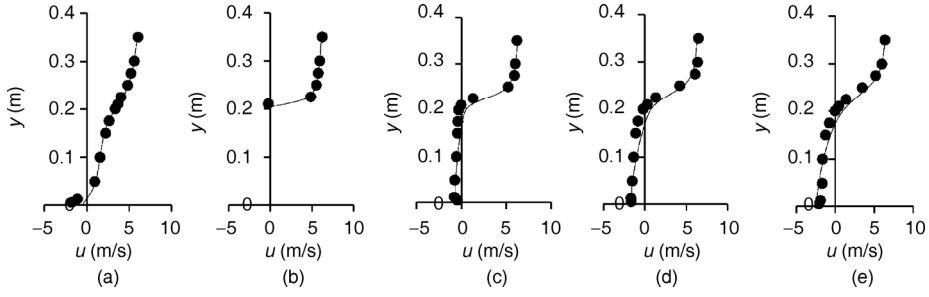

Fig. 5 Comparison of wind tunnel experimental data (dotted points) and RKE turbulence model results (solid lines) of mean streamwise wind velocity component u at (a) $x = -0.075$ m; (b) $x = 0$; (c) $x = 0.05$ m; (d) $x = 0.1$ m; (e) $x = 0.2$ m on a vertical plane along the centreline of the building

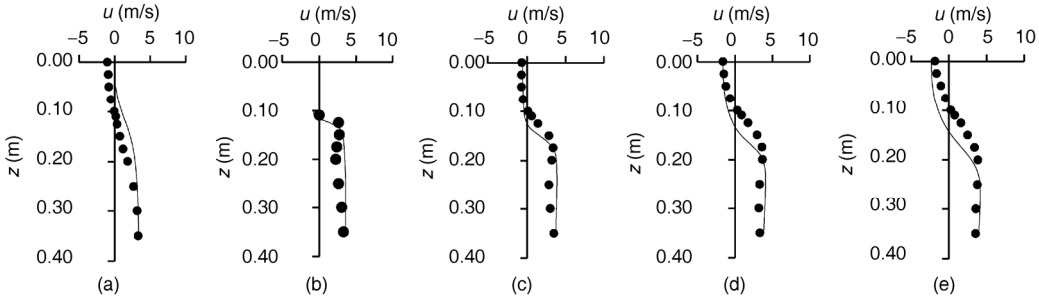

Fig. 6 Comparison of wind tunnel experimental data (dotted points) and RKE turbulence model results (solid lines) of mean streamwise wind velocity component u at (a) $x = -0.075$ m; (b) $x = 0$; (c) $x = 0.05$ m; (d) $x = 0.1$ m; (e) $x = 0.2$ m on a horizontal plane at $y = 0.0125$ m $\left(\frac{1}{16}h\right)$, for half domain

In the region outside the recirculation zones (generally, in the vertical direction this corresponds to the region at $y > 0.2$ m, while in the transverse direction it is in the region at $z < -0.1$ m and $z > 0.1$ m) results are predicted more closely than are in the region within the recirculations.

Comparison of the scalar wind velocity between the simulation results and the wind tunnel experimental data are shown in Figs. 7 and 8. Figures 7(a)–(e) compare the scalar wind velocity at various locations on a vertical plane along the centreline of the building, while Figs. 8(a)–(e) compare same wind velocity at similar locations on a horizontal plane at $y = 0.0125$ m, for half domain. As shown in the figures, the calculated scalar velocity profiles are also in very close agreement with the experimental data at nearly all the measuring points at both the front of and behind the building. Very good agreement was also obtained for the scalar velocity on the horizontal plane at $y = 0.0125$ m as shown in Figs. 8(a)–(e), except for the region within the recirculation zones.

Figure 9 compares the experimental and calculated scalar wind velocity on the horizontal plane at $y = 0.0125$ m $\left(\frac{1}{16}h\right)$ near the ground surface in order to quantify the performance and further assess the capability of RKE turbulence model in predicting the flow parameters for calculating ventilation indices at the location around the pedestrian height. It would be observed from the figure that for majority of the measuring points on this plane, particularly at the strong wind regions outside the recirculation zones, the calculated scalar wind velocity are within 15% error margin of the measured values. The margin of error, which corresponds to an accuracy of 85%, is considered adequate when it is noted that the error margin of 15% is normally reserved for and considered highly accurate for the region where the wind speed is accelerated (Janssen et al. 2013). In the weak-wind region, majority of the results are predicted within 20% error or 80% accuracy level. At this level of accuracy even at these weak-wind regions, the model is believed to have performed very well and is therefore quite adequate for calculating the air ventilation performance of the building configurations.

As demonstrated in the above validation, the current CFD k–ε turbulence model has performed quite well in predicting the flow field around the model of a single high-rise building. The approximate 15%–20% margin of error

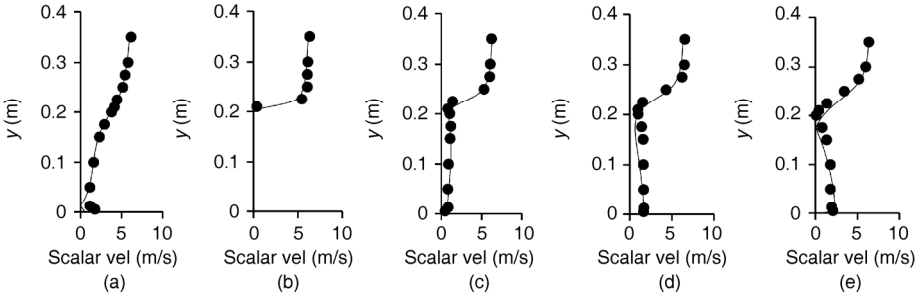

Fig. 7 Comparison of wind tunnel experimental data (dotted points) and the RKE turbulence model results (solid lines) of profiles of scalar wind velocity at (a) $x = -0.075$ m; (b) $x = 0$; (c) $x = 0.05$ m; (d) $x = 0.1$ m; (e) $x = 0.2$ m on a vertical plane along the centreline of the building

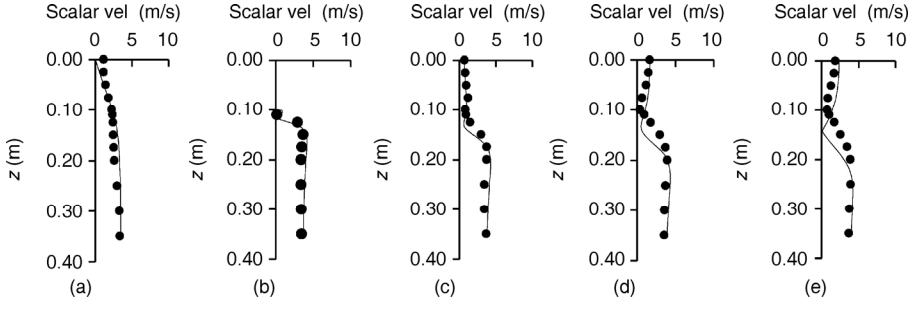

Fig. 8 Comparison of wind tunnel experimental data (dotted points) and the RKE turbulence model results (solid lines) of profiles of scalar wind velocity at (a) $x = -0.075$ m; (b) $x = 0$; (c) $x = 0.05$ m; (d) $x = 0.1$ m; (e) $x = 0.2$ m on a horizontal plane at $y = 0.0125$ m $\left(\frac{1}{16}h\right)$, for half domain

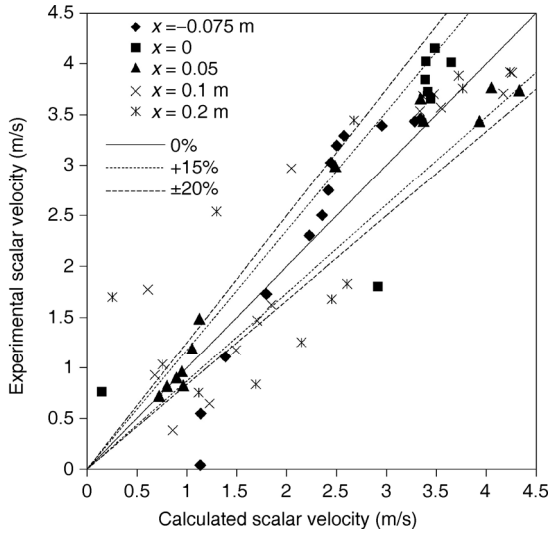

Fig. 9 Comparison of experimental scalar wind velocity data on a horizontal plane at y = 0.0125 m with calculated results

of the calculated scalar wind velocity values relative to the experimental data was within the acceptable margin in engineering tolerance (Cheung and Liu 2011). There is no doubt that some of the errors would be due to the assumption of isotropic turbulence stresses in the near-wall region made in the formulation of k–ε turbulence models. However, some of the errors could be due to interpolation inaccuracies for the flow and turbulence parameters at the inflow boundary. The conditions of the measurement procedures which cannot be completely replicated by the CFD calculations could have also contributed to the differences observed. Errors due to these factors can be eliminated or reduced for accurately specified inflow parameters and defined calculation conditions. Considering this performance and the computational resourcefulness of the k–ε model, it was believed that the model was robust enough for predicting the air ventilation performance in the two-building structure.

3 Numerical simulations

3.1 Configuration of the computational domain

The two-building apartments simulated consisted of a four-storey building with height H = 12 m representing a typical low-rise building, and a second building located upwind, with the height varied to assess the impact of height on wind flow around the low-rise building. The height of the upwind building was varied from H to 3H with a step increase of ½H, while the spacing distance S between the buildings was increased from ½H to 3H by the same step increase. The configuration in which no building was present upwind of the low-rise building was used as the reference case. Three different wind directions, θ_1 = 0° (wind direction perpendicular to the windward face of the upwind building), θ_2 = 22.5°, and θ_3= 45°, were investigated in order to examine the impact of wind direction on the air ventilation performance of the different configurations. The configuration and the geometry of the two-building structure, indicating the different directions of the approach wind flow considered, are as illustrated in Figs.10 and 11.

The computational domain was again designed according to the recommendations of major CFD guidelines. However,

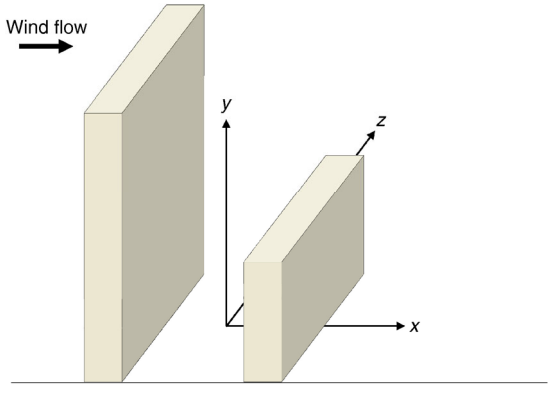

Fig. 10 Configuration of the two-building structure

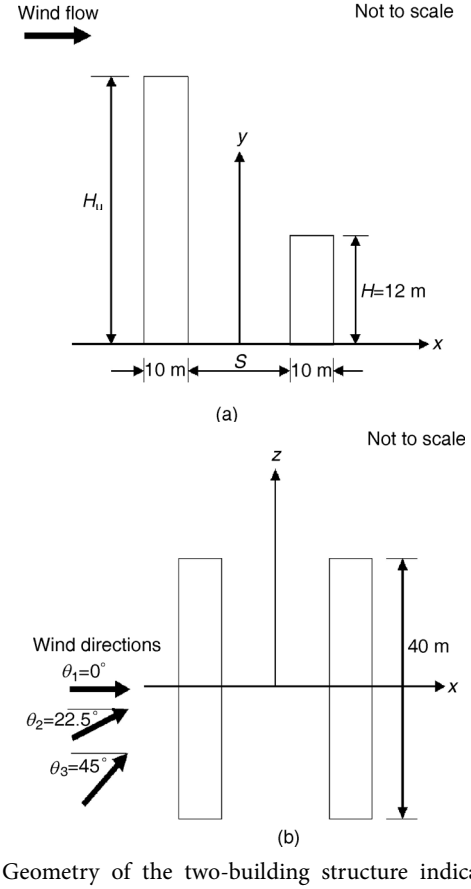

Fig. 11 Geometry of the two-building structure indicating the different directions of the approach wind flow: (a) side view; (b) top view

the height (H_u) of the upwind building was now used as the reference height. The domain was discretized into unstructured tetrahedral mesh elements using ANSYS Meshing 14.0, and it was ensured that the aspect ratios of the grid shapes were kept below 20 (ANSYS 2011). Grid sensitivity test was conducted for the different domain sizes used for the various configurations by repeatedly refining the grids for each of the domains until the prediction results from the last two consecutive grid systems was below 5%. The total number of mesh elements ranged from 1.5 million for the single low-rise building configuration as reference to 3.5 million for the configuration with the tallest building and greatest building separation. The vertical profile of the mean wind speed at the inflow boundary of the domain was represented by the logarithmic law with a roughness parameter. For a sub-urban residential area the corresponding roughness parameter y_0 is 0.5 m (Yim et al. 2009). However, in order to be able to locate the pedestrian evaluation height (2 m above ground surface) at the third or higher grid from the surface (Franke et al. 2004; Tominaga et al. 2008), a much smaller value (y_0 = 0.02 m) was assigned. In the Davenport roughness classification this corresponds to a terrain of grassland (Wieringa 1992). We have therefore assumed, in our study, a group of isolated two adjacent buildings. The reference wind speed, U = 0.92 m/s, which was the ten-year (2003–2012) average at a height of 10 m in Kuala Lumpur. The corresponding Reynolds number (Re_H) at the height of the low-rise building is well above the critical limit of 4000 (Uehara et al. 2003). The turbulent kinetic energy and the rate of dissipation of turbulent kinetic energy profiles at the inflow boundary were prescribed as follows (Richards and Hoxey 1993): $k(y) = u^{*2}_{ABL} / \sqrt{C_\mu}$; $\varepsilon(y) = u^{*3}_{ABL} / \kappa(y + y_0)$, where y is the height coordinate, u^*_{ABL} is the atmospheric boundary layer friction velocity, determined from the reference wind speed, $\kappa(\approx 0.4 - 0.42)$ is the von Karman constant, and $C_\mu(=0.09)$ is a model constant of the standard k–ε model. The lateral and top boundaries of the computational domain were assigned the slip wall conditions. At the downstream boundary the outflow boundary conditions were applied. The standard wall functions by Launder and Spalding (1974) were applied to model the flows in the near wall regions of the building walls and the ground surface. For the building walls the smooth surface conditions were applied, while on the ground surface the standard wall functions modified for roughness was employed. The standard wall function provides a means of evaluating flow variables at the wall adjacent cells from the wall values via the equivalent grain roughness height, K_s, for the boundary layer. In Fluent 6.3, the roughness height is related to the roughness length as

$$K_{s,ABL} = \frac{9.793 y_0}{C_s} \tag{5}$$

The relationship is used in evaluating the mean streamwise wind speed, the turbulent kinetic energy, and turbulent dissipation rate, respectively, at the wall adjacent cell as follows:

$$\frac{U_p u^*}{u_\tau^2} = \frac{1}{\kappa} \ln\left(\frac{E u^* y_p}{\nu\left(1 + C_s K_s^+\right)}\right) \tag{6}$$

$$k_p = \frac{u^{*2}}{\sqrt{C_\mu}} \tag{7}$$

$$\varepsilon_p = \frac{u^{*3}}{\kappa y_p} \tag{8}$$

where u^* and u_τ are two different wall function friction velocities, κ is von Karman constant (≈ 0.40 – 0.42), E is the empirical constant for a smooth wall (≈ 9.793), C_s is roughness constant, and K_s^+ is the dimensionless physical roughness height.

The mathematical models were simulated by employing the commercial CFD codes ANSYS Fluent 14.0. Computation was by the pressure-based solver and the SIMPLE scheme was adopted as the pressure–velocity coupling method. The second order discretization scheme was used for the pressure calculations, while the momentum, turbulent kinetic energy and rate of dissipation of turbulent kinetic energy equations were computed by the QUICK scheme. The scaled residuals for iteration convergence were dropped five orders of magnitude for all the variables. The CFD models were computed on a network of interconnected 8 CPU × 6 Nodes Quad-Core AMD Opteron™ Processor SunFire Systems of the CICT Unit of Universiti Teknologi Malaysia (UTM).

3.2 Air ventilation performance criteria

From the view point of human comfort and environmental health, air ventilation serves to maintain the quality of air in an environment, induce a sensation of physiological cooling, and in an environment with considerable thermal elevation, remove some of the heat content. The comfort factor which induces sensation of cooling is air movement, while the quality of air is dependent on the quantity of airflow between the environment and an external medium. In order to quantify the air ventilation impact of the various building configurations considered in this study, therefore, two air ventilation indicators were employed: the velocity ratio (VR) and air exchange rate (AER). The various heights of the upwind building considered are designated by a dimensionless parameter called height ratio (HR), defined

as the ratio of the height of the upwind building to that of the downwind building. The air ventilation indicators are discussed in the following sections.

3.2.1 Velocity ratio

The wind VR is an indicator used to compare pedestrian level wind availability around buildings. It takes into account the impacts of building configurations on wind flow, and is normally employed for outdoor air ventilation study. Quantitatively, it is defined according to Ng et al. (2008) and Yim et al. (2009) as follows:

$$\mathrm{VR} = V_\mathrm{p} / V_\infty$$

where, V_p is the wind velocity at the pedestrian level (2 m above ground surface) where air ventilation is being investigated, and V_∞ is a reference wind velocity. For this study, the reference wind velocity was taken as the wind velocity at the gradient height, which is the boundary layer height, at the buildings location, which is not affected by the ground surface roughness and other surface forcing (Yim et al. 2009). For the suburban terrain category under consideration, the gradient height is 390 m (Davenport 1960; Givoni 1998). The mean value of air velocity ratio was computed on the horizontal plane between the buildings, at 2 m height from the ground surface (pedestrian height) and spanning the width of the buildings. The location of the evaluation plane is shown in Fig. 12(a).

3.2.2 Air exchange rate

The concept of air exchange rate (AER) has been used in previous studies (Li et al. 2005; Liu et al. 2005; Xie et al. 2006b; Mirzaei and Haghighat 2010) to quantitatively compare air ventilation efficiency in 2-D street canyons. It denotes the volumetric air exchange per unit time and is based on the principle of mass conservation of incompressible flow across the air ventilation boundary into an objective canyon under investigation. Air entering into the canyon across the boundaries is denoted as positive AER (AER+), while that exiting is termed negative AER (AER–).

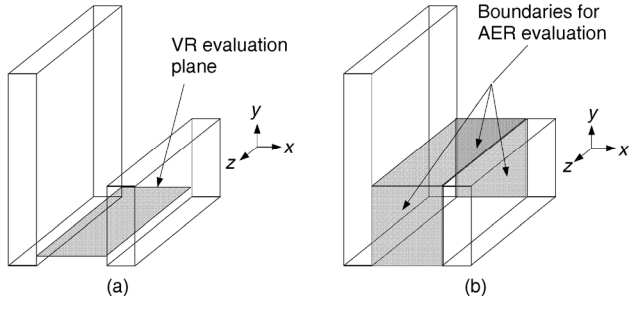

Fig. 12 Evaluation geometries for velocity ratio and air exchange rate

By the conservation principle, the magnitudes of the two AER components are equal. For the 3-D two-building system in the present study the air ventilation boundaries are as defined in Fig. 12(b). Following Xie et al. (2006), for the 3-D system, the time-dependent AER+ can be expressed by the ensemble average of the positive components of velocities at the boundaries as

$$\mathrm{AER+}(t) = \sum_{i=1}^{2}\int_0^T [\overline{W_+}(t,\Gamma) + w''_+(t,\Gamma)]\mathrm{d}t\Big|_{\mathrm{side}\,i} + \int_0^T [\overline{V_+}(t,\Gamma) + v''_+(t,\Gamma)]\mathrm{d}t\Big|_{\mathrm{Top}}$$

where, $\int_0^T [\overline{W_+}(t,\Gamma) + w''_+(t,\Gamma)]\mathrm{d}t$ and $\int_0^T [\overline{V_+}(t,\Gamma) + v''_+(t,\Gamma)]\mathrm{d}t$ are the ensemble averages of positive horizontal velocity on the two-side vertical boundaries, and the ensemble average of positive vertical velocity on the top horizontal boundary, respectively. The positive directions of flow are as indicated by the coordinate system shown in Fig. 12. The temporal average of AER+ can then be related to the time-dependent AER+ as

$$\begin{aligned}\overline{\mathrm{AER+}} &= \int_0^T \mathrm{AER+}(t)\mathrm{d}t \\ &= \sum_{i=1}^{2}\int_0^T\int_\Gamma [\overline{W_+}(t,\Gamma) + w''_+(t,\Gamma)]\mathrm{d}\Gamma\,\mathrm{d}t\Big|_{\mathrm{side}\,i} + \int_0^T\int_\Gamma [\overline{V_+}(t,\Gamma) + v''_+(t,\Gamma)]\mathrm{d}\Gamma\,\mathrm{d}t\Big|_{\mathrm{Top}} \\ &= \sum_{i=1}^{2}\int_\Gamma \Big(\int_0^T [\overline{W_+}(t,\Gamma) + w''_+(t,\Gamma)]\mathrm{d}t\Big)\mathrm{d}\Gamma\Big|_{\mathrm{side}\,i} + \int_\Gamma \Big(\int_0^T [\overline{V_+}(t,\Gamma) + v''_+(t,\Gamma)]\mathrm{d}t\Big)\mathrm{d}\Gamma\Big|_{\mathrm{Top}}\end{aligned}$$

Based on the conservation law discussed previously, we can write

$$\mathrm{AER+} = \sum_{i=1}^{2}\int_\Gamma \overline{W_+}\mathrm{d}\Gamma\Big|_{\mathrm{side}\,i} + \sum_{i=1}^{n}\frac{1}{2}\int_\Gamma \overline{w''w''}^{1/2}\mathrm{d}\Gamma\Big|_{\mathrm{side}\,i} + \int_\Gamma \overline{V_+}\mathrm{d}\Gamma\Big|_{\mathrm{Top}} + \frac{1}{2}\int_\Gamma \overline{v''v''}^{1/2}\mathrm{d}\Gamma\Big|_{\mathrm{Top}}$$

Assuming isotropic turbulence ($\overline{u''u''} = \overline{v''v''} = \overline{w''w''}$) at high Reynolds number street flow, which has been supported by empirical results (Kastner-Klein et al. 2001), we can write

$$k = (\overline{u''u''} + \overline{v''v''} + \overline{w''w''})/2 = \frac{3}{2}\overline{u''u''}\Big(\text{or}\ \ \frac{3}{2}\overline{v''v''} = \frac{3}{2}\overline{w''w''}\Big)$$

$$\overline{v''v''}^{1/2} = \sqrt{\frac{2}{3}k}\Big|_{\mathrm{Top}}\ ;\ \ \overline{w''w''}^{1/2} = \sqrt{\frac{2}{3}k}\Big|_{\mathrm{Sides}}$$

For the 3-D system, the temporal positive AER can, thus,

be expressed as

$$\overline{\mathrm{AER}+} = \sum_{i=1}^{2}\int_{\Gamma}\overline{W_{+}}\,\mathrm{d}\Gamma\Big|_{\text{side } i} + \int_{\Gamma}\overline{V_{+}}\,\mathrm{d}\Gamma\Big|_{\text{Top}} + \sum_{i=1}^{3}\frac{1}{\sqrt{6}}\int_{\Gamma}\sqrt{k}\,\mathrm{d}\Gamma\Big|_{\text{plane } i}$$

where, $\overline{W_{+}}$ and $\overline{V_{+}}$ are the mean positive transverse and vertical velocity components, w''_{+} and v''_{+} are the mean positive transverse velocity and vertical velocity fluctuations, and k the turbulent kinetic energy on the ventilation boundaries Γ. In order to be able to compare the breathing capacities of the different configurations studied, the AER values were non-dimensionalized by the volume of the 3-D space (Fig. 12(b)) between the buildings, and a time scale based on the height of the downwind building. It would be noted that the non-dimensionlizing volume parameter is not a constant but changes as the spacing distance between the buildings changes.

4 Results and discussion

4.1 Variation of air velocity ratio with buildings height ratio

The results of the air ventilation performance measured in terms of the wind velocity ratio of the various two-building configurations investigated are presented in Fig. 13. Figures 13(a)–(c), compare the variation of velocity ratio with height ratio for the different wind directions and spacing distances. The HR 0 indicated in the figures represents the reference case of isolated low-rise building. As would be seen in Fig. 13(a) for $\theta = 0°$ (perpendicular wind direction), the wind velocity ratio is the highest at HR 0 for all the spacing distances investigated. This indicates that the presence of the upwind building actually obstructs wind flow at the pedestrian level. It was also observed in the figure that the velocity ratio generally decreases with increase in building height ratio, but increases with the spacing distance. Velocity ratio was observed to decrease continuously with height ratio for all spacing distances except at S 24 m, HR 1.0.

At HR 1.0, the rate of increase of velocity ratio with spacing distance decreases until at S 24 m when the velocity ratio begins to drop from a maximum of 0.18 (average wind speed of about 0.27 m/s) with spacing distance. At HR $\geqslant 1.5$, the velocity ratio increases with spacing distance. This results in the velocity ratio increasing with height ratio for $1.0 \leqslant \mathrm{HR} \leqslant 1.5$, $S > 30$ m. In other words, for these configurations in which the height of the upwind building is greater than that of the downwind building, greater air movement is induced at the pedestrian level. The same behaviour was observed at S 6 m for $1.5 \leqslant \mathrm{HR} \leqslant 2.0$. These types of results have also been reported in previous studies (Baik et al. 2000; Xie et al. 2005; Wang and Huang 2006; Wang et al. 2006). The phenomenon was partly attributed to the number and strength of vortices formed, and their sizes and locations. The greater the number of vortices, especially with the weaker low-rotating ones located close to the ground surface, the weaker the wind velocity at the pedestrian level. When one or two main vortices are formed with the centre of the upper vortex located around the roof level, there is greater mass and momentum exchange in the vertical direction between the upper main recirculations and the mean flow. This results in greater pedestrian level wind velocity. This phenomenon was also observed in this study as explained in the following sections.

The flow patterns around the two buildings for HRs 1.0–2.0, S 24 m and 36 m are as shown in Fig. 14. The figures show that velocity ratio very much depends on the number, size, and location of the recirculations. The velocity ratio is also determined by the interaction of the recirculations, and that between the recirculations and the building surfaces. For example, the recirculation centre for the HR 1.5, S 36 m configuration (Fig. 14(e)) is very much higher than that of HR 1.0, S 36 m (Fig. 14(d)), as such the taller configuration was able to channel the faster moving air from above the top of the upwind building down to the pedestrian level and cause wind velocity at the level to be higher than that of

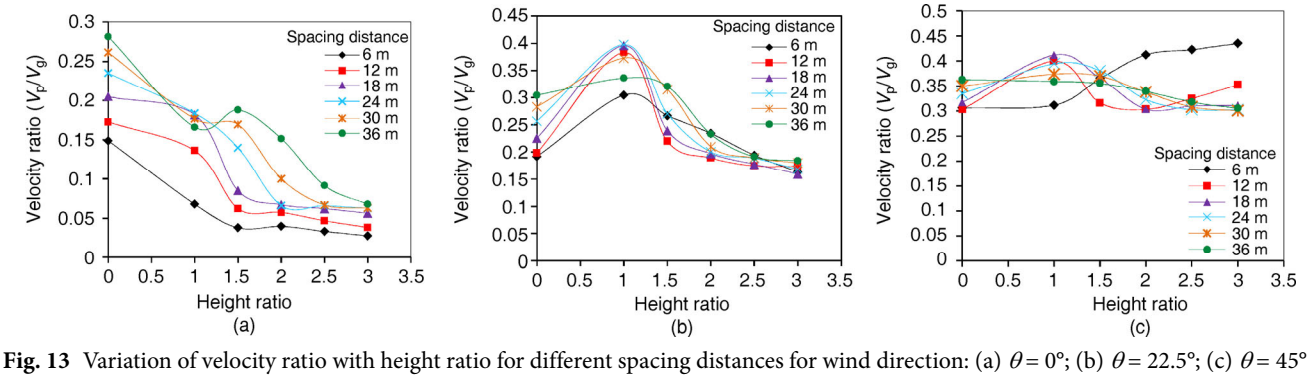

Fig. 13 Variation of velocity ratio with height ratio for different spacing distances for wind direction: (a) $\theta = 0°$; (b) $\theta = 22.5°$; (c) $\theta = 45°$

the HR 1.0 configuration. At *S* 36 m, it would be observed that even though the recirculation centre for the HR 2.0 configuration (Fig. 14(f)) appears to be higher than that of HR 1.5 (Fig. 14(e)), there is a backflow in the HR 2.0 configuration from the weaker recirculation behind the downwind building into the space between the two buildings, under the main recirculation. This caused the VR for the HR 2.0 configuration to be lower than that of the HR 1.5.

An inspection of building configurations HRs 1.0–2.0, *S* 24 m (Figs. 14(a)–(c)), shows continuously deteriorating conditions against the occurrence of higher pedestrian wind velocity as height ratio increases. In the HR 1.5 configuration (Fig. 14(b)) there is interaction of the main recirculation with much of the top surface of the downwind building. As such, even though the recirculation centre is higher than that of the HR 1.0 configuration (Fig. 14(a)), the pedestrian level wind velocity of the HR 1.0 configuration is higher. In the HR 2.0 configuration (Fig. 14(c)) there are two weak relatively smaller secondary recirculations close to the ground surface and a backflow from the recirculation behind the downwind building into the space between the two buildings. The double recirculation observed in Fig. 14(c) could be due to the greater height of the upwind building which channelled much faster moving air from above the roof level and recirculated at a relatively high speed. The slow moving air in-between the buildings and below the downwind building is now confined between the buildings. The momentum of the main recirculating now forces the air trapped against the leeward wall of the upwind building to begin to move downwards against the building wall, forming

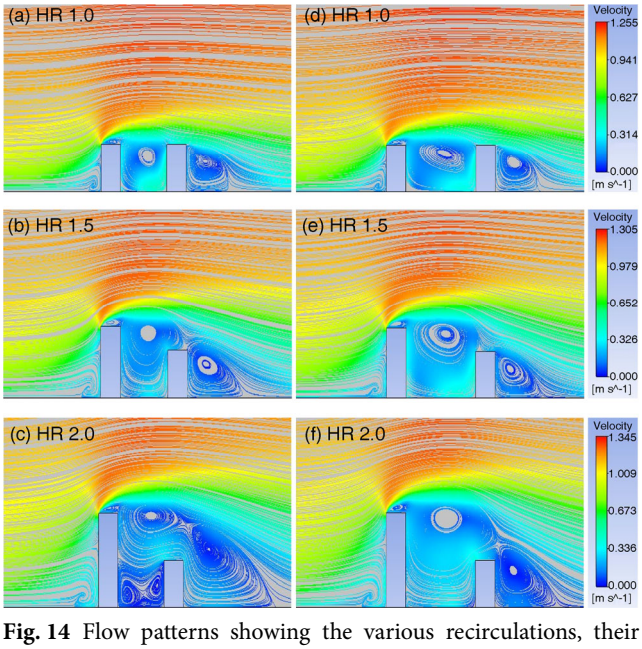

Fig. 14 Flow patterns showing the various recirculations, their relative sizes and locations for (a) – (c) *S* = 24 m, and (d) – (f) *S* = 36 m. Direction of flow is from left to right

an anticlockwise secondary vortex close to the ground, by the leeward wall surface of the upwind building. The air trapped against the windward wall of the downwind building is dragged by the momentum of the recirculating flow. It is aided by the ground flow of the secondary vortex to begin to move upwards against the windward wall of the downwind building, forming an opposite anticlockwise secondary vortex by the wall of the building. These adverse flow phenomena combine to weaken the pedestrian level wind velocity of the HR 2.0 configuration below that of HR 1.5. Lateral flows also appear to play a very significant role in determining the velocity ratio at the pedestrian level. For example, even though the recirculation centre for the HR 1.0, *S* 24 m configuration (Fig. 14(a)) is lower than that of HR 1.0, *S* 36 m (Fig. 14(d)), the average velocity ratio for the narrower configuration is higher. For HR $\geqslant$ 1.0, the maximum VR was found to be around 0.188, and this occurred at HR 1.5. There appears to be a limiting minimum value of VR for each spacing distance as the HR approaches higher values.

The highest VRs, ranging of 0.152 $\leqslant$ VR $\leqslant$ 0.188 (average wind speed between 0.22 and 0.27 m/s), occur for configurations 1.0 $\leqslant$ HR $\leqslant$ 2.0, *S* 36 m; 1.0 $\leqslant$ HR $\leqslant$ 1.5, *S* 30 m; and HR 1.0, *S* 24 m. At HR 1.0, spacing distances 24 m, 30 m, and 36 m give comparable values of wind velocity ratios for the height ratio, with spacing distance 24 m having the highest value of 0.184, which is about 22% reduction from that of the reference case. The 24 m spacing distance maintains this maximum VR for 1.0 $\leqslant$ HR $\leqslant$ 1.25. At HR 1.5 the maximum VR occurs at *S* 36 m. But between HRs 1.25 and 1.5, spacing distance 30 m gives velocity ratio values comparable to the value at HR 1.5, *S* 36 m. Beyond HR 1.5, VR curves for the various spacing distances dip sharply, such that only the 36 m spacing distance yields a VR of 0.152. Beyond HR 2.0, the curves continue to slide downwards, producing VR values much lower than 2.0. Just like there occurs an inflection at *S* 30 m and HR between 1.0 and 2.5, and a maximum at HR 1.5, *S* 36 m at which the highest natural ventilation condition is attained, it is reasonable to project that at higher spacing distances ($\gg$36 m) there would also occur equivalent maxima at higher height ratios, at which the best natural ventilation conditions would occur. However, further investigation is needed to confirm this reasoning. Such a study would provide wind flow and ventilation behaviours of the various building configurations at these greater spacing distances.

For wind flow at $\theta = 22.5°$ (Fig. 13(b)), the curves generally follow the same pattern. Unlike in the case of the perpendicular wind direction, the maximum VR does not occur at HR 0 when there is no building upwind of the low-rise building, but generally occurs at around HR 1.0 for all spacing distances. This suggests the occurrence of wind channelling along the axis of the passage between the

buildings. This phenomenon has been observed in previous studies (Blocken et al. 2007; Blocken et al. 2008; Yim et al. 2009) in which the increased wind speed in the passages between buildings were reported and attributed to the so called Venture-effect—wind speed increasing due to decrease in passage flow section. Figure 15 illustrates the differences between the flow pattern around the isolated building (Fig. 15(a)) and those around the HR 1.0–HR 2.0, *S* 24 m two-building configurations (Figs.15(b)–(d)). The increased wind flow effect can be observed in the space between the buildings, which is absent in the case of the isolated building. It could also be observed that the wind velocity and the area affected decrease with increase in height ratio. This is also reflected in the velocity ratio versus height ratio graph of Fig. 13(b). For HR > 1.0 velocity ratio decreases with increase in height ratio. However, for HR > 2.0, there is no significant difference in the velocity ratio for all the spacing distances, which now continues to decrease very gradually with height ratio.

It was also observed in Fig. 13(b) that at HR 1.0, the wind velocity ratio increases with increase in spacing distance, the rate of increase decreasing until VR 0.4 (average wind speed of 0.58 m/s) is reached at *S* 24 m, after which the velocity ratio began to fall with further increase in spacing distance. In other words, the channelling effect increases from *S* 6 m up to a maximum at *S* 24 and begins to decrease with further increase in spacing distance. This could mean that at very low spacing distances, there is a "wall effect" (Yim et al. 2009) of the sides of the two buildings, blocking much of the flow and preventing channelling. But at higher spacing distances, blockage is eased for more flow and channelling becomes more effective. As the spacing distance increases above 24 m, there is a decreasing influence of the channelling effect, resulting in reduced wind flow. At these greater spacing distances, the blockage effect of the upwind building begins to influence the wind flow on the downwind building. For the wind direction, the velocity ratios range between 0.17 and 0.4 (average wind speeds between 0.25 and 0.58 m/s), which are much greater than those obtained for wind direction θ = 0°. The velocity ratio is generally higher for θ = 22.5° than for θ = 0°.

The variation of velocity ratio with height ratio for wind direction θ = 45° is shown in Fig. 13(c). The same channelling effect is observed to occur at around HR 1.0 for all spacing distances except at 6 m, after which the interference effect becomes dominant at higher height ratios. The flow patterns around the isolated building and those around the HR 1.0–HR 2.0, *S* 24 m two-building configurations are as shown in Fig. 16. The same increased wind flow effect observed in the θ = 22.5° configurations can also be seen here, except that the velocity increase is much higher and the areas between the buildings affected are larger than those for the 22.5° configurations. The behaviour of the *S* 6 m curve deviates from those of others; it doesn't exhibit significant channelling at HR 1.0, but shows increase in the velocity ratio with height ratio beginning from HR 1.0. The reason for this is not immediately known, but it may be due to the influence of lateral flows. Compared to the cases for wind directions θ = 0° and θ = 22.5°, the range of values between the smallest and the highest velocity ratios is very small (0.3 ⩽ VR ⩽0.4)—average wind speeds between 0.44 and 0.58 m/s.

It would be noted that for the inclined wind directions, the VR is peaked at HR 1.0, unlike in the case of the perpendicular wind direction. For wind flow perpendicular to the windward face of the upwind building, the formation of a recirculating vortex and the vertical position of the vortex are the main mechanisms by which increased wind flow can occur at the pedestrian level of the cavity between two adjacent buildings of unequal heights. For an inclined wind flow, recirculation is mainly on a horizontal plane (see Figs. 15 and 16), and can therefore not induce a higher

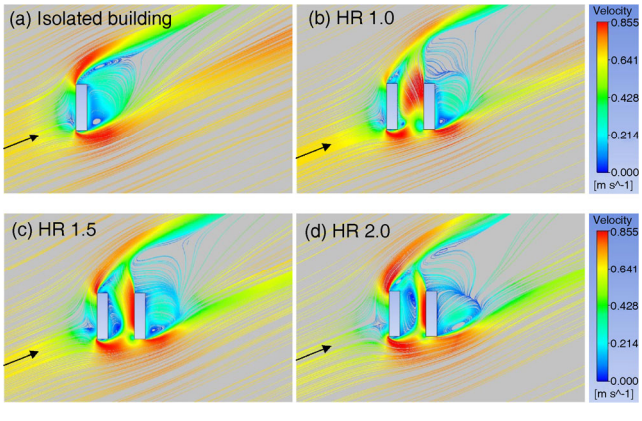

Fig. 15 Flow patterns showing the increased pedestrian level wind flow velocity between the two adjacent buildings at *S* = 24 m and for θ = 22.5°. The arrows indicate the direction of flow

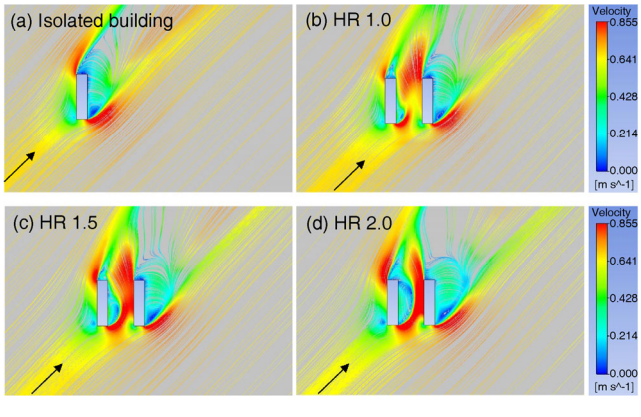

Fig. 16 Flow patterns showing the increased pedestrian level wind flow velocity between the two adjacent building at *S* = 24 m and for θ = 45°. The arrows indicate the direction of flow

wind flow at the pedestrian level. A higher upwind building serves to further block wind flow into the cavity, and hence the observed decrease of VR with increase in height ratio for these inclined directions.

4.2 Variation of dimensionless air exchange rate with height ratio

The results of the dimensionless air exchange rate for the various two-building configurations investigated are presented in Fig. 17. Figures 17(a), (c), and (e) compare the variation of dimensionless AER with HR for the various spacing distances for wind directions $\theta = 0°$, 22.5°, and 45°, respectively. Figures 17(b), (d), and (f) are the enlarged views of Figs. 17(a), (c), and (e), respectively, for HR $\geqslant$ 1.0 since curves are not distinctly indicated in Figs. 17(a), (c), and (e) for HR $\geqslant$ 1.0. Generally, as shown in Figs. 17(a), (c), and (e), the AER at HR 0 are higher than their equivalent at HR $\geqslant$ 1.0. This is unlike in the case of VR curves where it was shown that for $\theta = 22.5°$ and 45°, the velocity ratios were not necessarily highest at HR 0. Figures 17(a) and (b) indicate that for wind direction $\theta = 0°$, more air is induced as the spacing distance between the buildings increases. As shown in Fig.17(b), at S 6 m and 1.5 $\leqslant$ HR $\leqslant$ 2.0, AER increases with the height ratio, whereas it decreases with the height ratio at higher spacing distances. In the equivalent VR curves (Fig.13(a)), the velocity ratio increases with the height ratio both at S 6 m, 1.5 $\leqslant$ HR $\leqslant$ 2.0, and for S > 30 m, 1.0 $\leqslant$ HR $\leqslant$ 1.5. This indicates that for S > 30 m, 1.0 $\leqslant$ HR $\leqslant$ 1.5, even though greater air movement is induced at the pedestrian level as HR increases, less wind flow is actually entering into the 3-D space between the buildings at height > 2 m (the pedestrian height). This may be because the AER values were calculated for the entire 3-D space as against the pedestrian level averaging that was done for velocity ratio. Some configurations, such as encountered above, probably enable more flow into the 3-D cavity at the ground level by lateral flow phenomenon, than is admitted into the cavity at higher levels by both lateral and vertical flow exchanges. Since the pedestrian level wind flow is the main focus of the study, the performance as indicated by VR should be more representative of the ventilation behaviour at the pedestrian level. The maximum AER of 0.193 (airflow rate of 219.34 m^3/s) occurs at HR 1.0, S 30 m. At this height ratio the minimum AER is 0.155 (35.24 m^3/s), and it occurs at S 6 m. At HR 1.5, the equivalent minimum spacing distance to attain this level of AER is S 18 m, while HR 2.0, 2.5, and 3 require S > 24 m, 30 m and 36 m, respectively. For HR $\geqslant$ 1.5, S 36 m gives the highest AER values.

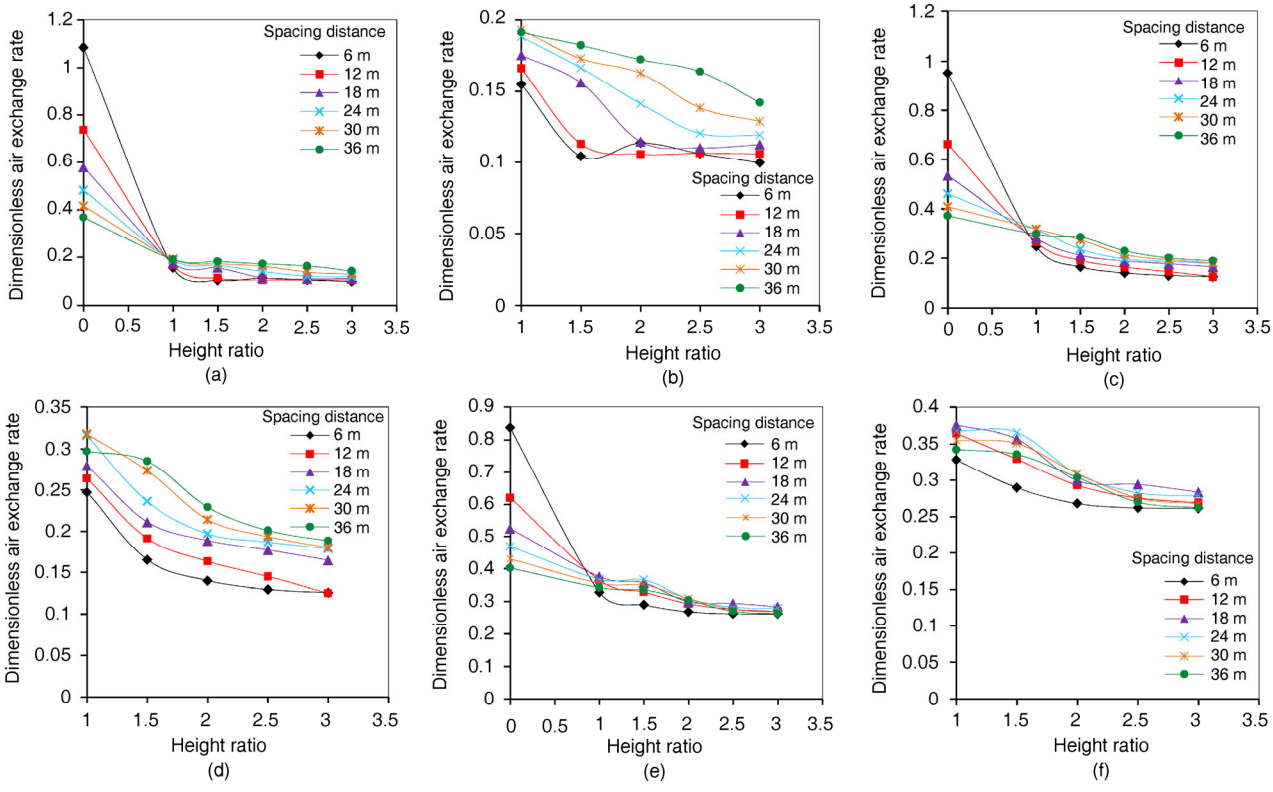

Fig. 17 Variation of dimensionless air exchange rate with height ratio for different spacing distances for wind direction: (a) $\theta = 0°$; (c) $\theta = 22.5°$; (e) $\theta = 45°$; (b), (d) & (f) are the enlarged views of (a), (c), & (e), respectively

For wind direction $\theta = 22.5°$ (Figs. 17(c) and (d)), AER generally decreases with increase in HR, but increases as the spacing distance increases. The maximum AER of 0.318 occurs at HR 1.0, *S* 30 m. This is closely followed by an AER value of 0.316 at *S* 24 m. At HR 1.5, $S > 24$ m is required to achieve the same level of AER as obtained at *S* 6 m for HR 1.0, while for HR > 2.0, $S > 36$ m is required. A spacing distance of 18 m at HR 2.5 gives the same level of AER as the maximum value of 0.193 recorded in the $\theta = 0°$ configuration at HR 1.0, *S* 30 m.

For wind direction $\theta = 45°$ (Figs. 17(e) and (f)), it was observed that at HR 1.0 the rate of increase of dimensionless AER with spacing distance decreases until the maximum AER of 0.376 was reached at *S* 18 m after which the AER began to fall with further increase in the spacing distance. The same trend was observed at HR 1.5 and HR 2.0 but with the maximum AERs of 0.366 and 0.309 reached at spacing distances 24 m and 30 m, respectively. This behaviour may also be due to flow channelling at HRs 1.0, 1.5 and 2.0, but whose influence decreases at *S* 18 m, 24 m, and 30 m, respectively. It was also observed that for HR $\geqslant$ 2.5 there were no significant differences between the dimensionless AERs. At HR 1.0 the minimum dimensionless AER of 0.328 occurred at S 6 m. The minimum dimensionless AER which was 0.261 and which occurred at HR 3.0, *S* 6 m, was greater than the maximum dimensionless AER of 0.193 for wind direction $\theta = 0°$.

Results presented so far are based on simplified two-block rectangular building configuration, neglecting the effects of architectural elements, such as balcony and non-flat roof shapes. The effects of the elements are rather complicated because of the diverse shapes and configurations, with the building structure, and the complicated vortex structures that they induced (Rahmatmand et al. 2014). But generally it has been reported that balconies can enhance wind flow into the indoor environment by developing higher positive pressures at the windward facade of a building, and by scooping outdoor air into the indoor space (Mohamed et al. 2008; Cui et al. 2013; Montazeri and Blocken 2013). Building roofs can also be designed to enhance ventilation around the building (Yassin 2011). Based on these functionalities of the architectural features, in the realistic urban setting, the results obtained by this study for ventilation in the outdoor environment of the rectangular building blocks represent the worst case scenarios.

5 Summary and conclusions

The influence of adjacent upwind building on air ventilation in a two-building configuration for the purpose of harnessing the full ventilation potential of the local wind conditions at the pedestrian level has been investigated numerically. The air ventilation criteria adopted in the study, in many areas, produced results that showed similar trend of the effects of spacing distance, height ratio and wind direction in the two-building configuration in which a taller building was situated at an upwind location of a low-rise building. It was shown that for wind flow in the perpendicular direction, the level of natural ventilation provided between the buildings depends on the number, sizes, and locations of the recirculations. It also depends on the interactions between the recirculations and the building surfaces, and the lateral wind flow induced along the axis of the passage between the buildings. All these factors determine the effectiveness of the building configuration in channelling the faster moving air from above the top of the buildings down to the pedestrian level. This shows why 2-D simulations cannot yield results that are representative of the actual phenomenon, as it cannot capture these turbulent flow features. For the wind direction, wind flow and air ventilation generally tend to decrease with increase in height ratio, and increase with increase in spacing distance when the upwind building is much higher than the downwind building. It was established, however, that at lower height ratios air ventilation increases with increase in height ratio after a certain maximum spacing distance, and decreases with increase in spacing distance. For such cases, the higher the upwind building or the smaller the spacing distance, the more is the wind flow and air ventilation that would be induced at the pedestrian level. The configurations of the buildings layout under this condition yield the best possible natural ventilation availability. It is projected that at higher spacing distances, this phenomenon could also occur for higher height ratios to yield the optimum natural ventilation conditions.

It was shown that the highest VRs, ranging from $0.152 \leqslant VR \leqslant 0.188$ (average wind speeds between 0.22 and 0.27 m/s), occur for configurations $1.0 \leqslant HR \leqslant 2.0$, *S* 36 m; $1.0 \leqslant HR \leqslant 1.5$, *S* 30 m; and HR 1.0, *S* 24 m. This range of wind speeds is well above the indoor air speed range of 0.1–1.5 m/s needed for a satisfactory thermal comfort conditions (Ismail 1996). Judging from the fact that the velocity ratio values are the maximum attainable as a result of the upwind building interference, the corresponding configurations are suggested as the preferred configurations when laying out buildings in this manner. As such, 24 m spacing distance is proposed for configurations $1.0 \leqslant HR \leqslant 1.25$, while for $1.25 < HR \leqslant 1.5$, the 30 m spacing distance is recommended. For HRs between 1.5 and 2, the 36 m spacing distance is suggested, while for HR > 2.0 the spacing distance needs to be greater than 36 m.

The inclined wind flow configurations ensure much greater air motions and ventilation at the pedestrian level. This is as a result of the channelling phenomenon which is very dominant at lower height ratios and spacing distances.

For the low-wind environment studied, the maximum air motions induced at the buildings outdoor by the channelling effects in the inclined wind configurations are not enough to constitute wind nuisance. However, in high-wind regions, it would be necessary to examine the level of air motion induced by the different wind directions by the channelling effect in order to avoid unacceptable air motions at the pedestrian level. The exact choice of the spacing distance depends on the various activities in and around the environment.

This study represents the first time a 3-D CFD numerical simulation would be undertaken using actual wind data and real-scale building dimensions to determine appropriate separation distances between buildings for various configurations of the buildings layout for use in developing guidelines for building layout, though simple configurations of the building structures was used. From the view point of human comfort and environmental health in low-wind environments, if a high-rise building is to be located upwind and close to a building with a lower height, the appropriate spacing distances as discussed in the preceding section need to be considered in the building design. The findings of this research work could contribute to passive enhancement of the comfort and health conditions of indoor inhabitants and those around the pedestrian areas. However, more investigations are needed to study the numerous other configurations of the two-building structure and arrays of buildings in order to make the findings more comprehensive for drawing up building design guidelines with a consideration for thermal comfort and environmental health based on natural ventilation. Greater spacing distances are also needed to be investigated for higher height ratios for their maximum natural ventilation availability.

Acknowledgements

The authors would like to thank the CICT Unit of Universiti Teknologi Malaysia (UTM) for providing the computational support for conducting the research. They also express much appreciation to the anonymous reviewers for their valuable comments which helped to improve the paper. The first author also wishes to acknowledge Federal University of Technology Minna, Nigeria, and TETFund for providing the support and Study Fellowship for the research programme.

References

Allard F, Ghiaus C (2005). Natural Ventilation in the Urban Environment Assessment and Design. London: Earthscan.

Ansys (2011). ANSYS Release 14.0. User's Guide. Canonsburg, PA, USA: ANSYS Inc.

Baik J-J, Kim J-J (1999). A numerical study of flow and pollutant dispersion characteristics in urban street canyons. *Journal of Applied Meteorology*, 38: 1576–1589.

Baik J-J, Park R-S, Chun H-Y, Kim J-J (2000). A laboratory model of urban street-canyon flows. *Journal of Applied Meteorology*, 39: 1592–1600.

Blocken B, Carmeliet J, Stathopoulos T (2007). CFD evaluation of wind speed conditions in passages between parallel buildings—Effect of wall-function roughness modifications for the atmospheric boundary layer flow. *Journal of Wind Engineering and Industrial Aerodynamics*, 95: 941–962.

Blocken B, Stathopoulos T, Carmeliet J (2008). Wind environmental conditions in passages between two long narrow perpendicular buildings. *Journal of Aerospace Engineering*, 21: 280–287.

Bottema M (1993). Wind Climate and Urban Geometry. Eindhoven, the Netherlands: Technische Universiteit Eindhoven.

Bourbia F, Boucheriba F (2010). Impact of street design on urban microclimate for semi arid climate (Constantine). *Renewable Energy*, 35: 343–347.

Brixey LA, Heist DK, Richmond-Bryant J, Bowker GE, Perry SG, Wiener RW (2009). The effect of a tall tower on flow and dispersion through a model urban neighborhood: Part 2. Pollutant dispersion. *Journal of Environmental Monitoring*, 11: 2171–2179.

Buccolieri R, Sandberg M, Di Sabatino S (2010). City breathability and its link to pollutant concentration distribution within urban-like geometries. *Atmospheric Environment*, 44: 1894–1903.

Cheng WC, Liu C-H, Leung DYC (2008). Computational formulation for the evaluation of street canyon ventilation and pollutant removal performance. *Atmospheric Environment*, 42: 9041–9051.

Cheung JOP, Liu C-H (2011). CFD simulations of natural ventilation behaviour in high-rise buildings in regular and staggered arrangements at various spacings. *Energy and Buildings*, 43: 1149–1158.

Cui DJ, Mak CM, Niu JL (2013). Effect of balconies and upper-lower vents on ventilation and indoor air quality in a wind-induced, naturally-ventilated building. *Building Services Engineering Research and Technology*, 35: 393–407.

Davenport AG (1960). Wind loads on structures. Technical Paper No. 88. Ottawa, Canada: National Research Council.

DePaul FT, Sheih CM (1985). A tracer study of dispersion in an urban street canyon. *Atmospheric Environment* (*1967*), 19: 555–559.

Fenger J (1999). Urban air quality. *Atmospheric Environment*, 33: 4877–4900.

Franke J (2006). Recommendations of the COST action C14 on the use of CFD in predicting pedestrian wind environment. In: Proceedings of 4th International Symposium on Computational Wind Engineering, Yokohama, Japan, pp. 529–532.

Franke J, Hellsten A, Schlünzen H, Carissimo B (2007). Best practice guideline for the CFD simulation of flows in the urban environment. COST Action 732, Quality Assurance and Improvement of Microscale Meteorological Models. Brussels, COST Office.

Franke J, Hirsch C, Jensen AG, Krüs HW, Schatzmann M, Westbury PS, Miles SD, Wisse JA, Wright NG (2004). Recommendations on the use of CFD in wind engineering. In: van Beeck JPAJ (Ed.),

Proceedings of International Conference on Urban Wind Engineering and Building Aerodynamics, COST Action C14, Impact of Wind and Storm on City Life Built Environment, Sint-Genesius-Rode, Belgium.

Gao Y, Yao R, Li B, Turkbeyler E, Luo Q, Short A (2012). Field studies on the effect of built forms on urban wind environments. *Renewable Energy*, 46: 148–154.

Givoni B (1998). Climate considerations in building and urban design, New York: Van Nostrand Reinhold.

Gu Z-L, Zhang Y-W, Cheng Y, Lee S-C (2011). Effect of uneven building layout on air flow and pollutant dispersion in non-uniform street canyons. *Building and Environment*, 46: 2657–2665.

Hang J, Li Y, Sandberg M, Buccolieri R, Di Sabatino S (2012). The influence of building height variability on pollutant dispersion and pedestrian ventilation in idealized high-rise urban areas. *Building and Environment*, 56: 346–360.

Heist DK, Brixey LA, Richmond-Bryant J, Bowker GE, Perry SG, Wiener RW (2009). The effect of a tall tower on flow and dispersion through a model urban neighborhood: Part 1. Flow characteristics. *Journal of Environmental Monitoring*, 11: 2163–2170.

Ismail AM. (1996). Wind-driven natural ventilation in high-rise office buildings with special reference to the hot-humid climate of Malaysia. Cardiff University.

Janssen W, Blocken B, Van Hooff T (2013). Pedestrian wind comfort around buildings: Comparison of wind comfort criteria based on whole-flow field data for a complex case study. *Building and Environment*, 59: 547–562.

Ji W, Zhao B (2014). Numerical study of the effects of trees on outdoor particle concentration distributions. *Building Simulation*, 7: 417–427.

Kastner-Klein P, Fedorovich E, Rotach MW (2001). A wind tunnel study of organised and turbulent air motions in urban street canyons. *Journal of Wind Engineering and Industrial Aerodynamics*, 89: 849–861.

Kim J-J, Baik J-J (1999). A numerical study of thermal effects on flow and pollutant dispersion in urban street canyons. *Journal of Applied Meteorology*, 38: 1249–1261.

Krüger E, Minella F, Rasia F (2011). Impact of urban geometry on outdoor thermal comfort and air quality from field measurements in Curitiba, Brazil. *Building and Environment*, 46: 621–634.

Launder BE, Spalding DB (1974). The numerical computation of turbulent flows. *Computer Methods in Applied Mechanics and Engineering*, 3: 269–289.

Li QS, Fang JQ, Jeary AP, Wong CK (1998). Full scale measurements of wind effects on tall buildings. *Journal of Wind Engineering and Industrial Aerodynamics*, 74–76: 741–750.

Li X-X, Liu C-H, Leung DYC (2005). Development of a k–ε model for the determination of air exchange rates for street canyons. *Atmospheric Environment*, 39: 7285–7296.

Li X-X, Liu C-H, Leung DYC (2009). Numerical investigation of pollutant transport characteristics inside deep urban street canyons. *Atmospheric Environment*, 43: 2410–2418.

Li X-X, Liu C-H, Leung DYC, Lam KM (2006). Recent progress in CFD modelling of wind field and pollutant transport in street canyons. *Atmospheric Environment*, 40: 5640–5658.

Liu C-H, Leung DYC, Barth MC (2005). On the prediction of air and pollutant exchange rates in street canyons of different aspect ratios using large-eddy simulation. *Atmospheric Environment*, 39: 1567–1574.

Maruyama T, Ishizaki H (1988). A wind tunnel test on the boundary layer characteristics above an urban area. *Journal of Wind Engineering and Industrial Aerodynamics*, 28: 139–148.

Mirzaei PA, Haghighat F (2010). A novel approach to enhance outdoor air quality: Pedestrian ventilation system. *Building and Environment*, 45: 1582–1593.

Mohamed M, Prasad D, Tahir MM (2008). A study on balcony and its potential as an element of ventilation control in naturally ventilated apartment in hot and humid climate. In: Proceedings of International Conference on Construction and Building Technology (ICCBT), Kuala Lumpur, Malaysia, pp. 173–180.

Montazeri H, Blocken B (2013). CFD simulation of wind-induced pressure coefficients on buildings with and without balconies: Validation and sensitivity analysis. *Building and Environment*, 60: 137–149.

Ng E, Katzschner L, Wang U, Ren C, Chen L (2008). Draft urban climatic analysis map—Urban climatic map and standards for wind environment—Feasibility study. Working Paper No. 1A. Technical Report for Planning Department HKSAR. Report No. WP1A. Planning Department of Hong Kong Government.

Ogawa Y, Oikawa S (1982). A field investigation of the flow and diffusion around a model cube. *Atmospheric Environment* (*1967*), 16: 207–222.

Oke TR (1988). Street design and urban canopy layer climate. *Energy and Buildings*, 11: 103–113.

Panagiotou I, Neophytou MK-A, Hamlyn D, Britter RE (2013). City breathability as quantified by the exchange velocity and its spatial variation in real inhomogeneous urban geometries: An example from central London urban area. *Science of the Total Environment*, 442: 466–477.

Popescu CG (2011). Relation between vehicle traffic and heavy metals content from the particulate matters. *Romanian Reports in Physics*, 63: 471–482.

Rahmatmand A, Yaghoubi M, Rad E, Tavakol M (2014). 3D experimental and numerical analysis of wind flow around domed-roof buildings with open and closed apertures. *Building Simulation*, 7: 305–319.

Richards PJ, Hoxey RP (1993). Appropriate boundary conditions for computational wind engineering models using the k–ε turbulence model. *Journal of Wind Engineering and Industrial Aerodynamics*, 46: 145–153.

Shih TH, Liou WW, Shabbir A, Yang Z, Zhu J (1995). A new k–ε eddy viscosity model for high reynolds number turbulent flows. *Computers & Fluids*, 24: 227–238.

Sini J-F, Anquetin S, Mestayer PG (1996). Pollutant dispersion and thermal effects in urban street canyons. *Atmospheric Environment*, 30: 2659–2677.

Tominaga Y, Mochida A, Shirasawa T, Yoshie R, Kataoka H, Harimoto K, Nozu T (2004). Cross comparisons of CFD results of wind environment at pedestrian level around a high-rise building and within a building complex. *Journal of Asian Architecture and Building Engineering*, 3: 63–70.

Tominaga Y, Mochida A, Yoshie R, Kataoka H, Nozu T, Yoshikawa M, Shirasawa T (2008). AIJ guidelines for practical applications of CFD to pedestrian wind environment around buildings. *Journal of Wind Engineering and Industrial Aerodynamics*, 96: 1749–1761.

Ubbl (2006 Amendment). Malaysia Uniform Building By-Laws 1984. Kuala Lumpur: MDC Publishers.

Uehara K, Murakami S, Oikawa S, Wakamatsu S (2000). Wind tunnel experiments on how thermal stratification affects flow in and above urban street canyons. *Atmospheric Environment*, 34: 1553–1562.

Uehara K, Wakamatsu S, Ooka R (2003). Studies on critical Reynolds number indices for wind-tunnel experiments on flow within urban areas. *Boundary-Layer Meteorology*, 107: 353–370.

Van Hooff T, Blocken B (2010). Coupled urban wind flow and indoor natural ventilation modelling on a high-resolution grid: A case study for the Amsterdam ArenA stadium. *Environmental Modelling & Software*, 25: 51–65.

Wang J-S, Huang Z (2006). Numerical study on flow and dispersion in rban street canyons of asymmetrical configurations. *Journal of Hydrodynamics, Ser. B*, 18(Suppl.): 146–150.

Wang J-S, Zhao B-Q, Ye C, Yang D-Q, Huang Z (2006). Optimizing layout of urban street canyon using numerical simulation coupling with mathematical optimization. *Journal of Hydrodynamics, Ser. B*, 18(Suppl.): 345–351.

Wieringa J (1992). Updating the Davenport roughness classification. *Journal of Wind Engineering and Industrial Aerodynamics*, 41: 357–368.

Xie S, Zhang Y, Qi L, Tang X (2003). Spatial distribution of traffic-related pollutant concentrations in street canyons. *Atmospheric Environment*, 37: 3213–3224.

Xie X, Huang Z, Wang J (2005). Impact of building configuration on air quality in street canyon. *Atmospheric Environment*, 39: 4519–4530.

Xie X, Huang Z, Wang J (2006a). The impact of urban street layout on local atmospheric environment. *Building and Environment*, 41: 1352–1363.

Xie X, Liu C-H, Leung DY, Leung MK (2006b). Characteristics of air exchange in a street canyon with ground heating. *Atmospheric Environment*, 40: 6396–6409.

Yassin MF (2011). Impact of height and shape of building roof on air quality in urban street canyons. *Atmospheric Environment*, 45: 5220–5229.

Yim SHL, Fung JCH, Lau AKH, Kot SC (2009). Air ventilation impacts of the "wall effect" resulting from the alignment of high-rise buildings. *Atmospheric E nvironment*, 43: 4982–4994.

Yuan C, Ng E, Norford LK (2014). Improving air quality in high-density cities by understanding the relationship between air pollutant dispersion and urban morphologies. *Building and Environment*, 71: 245–258.

Zain ZM, Taib MN, Baki SMS (2007). Hot and humid climate: prospect for thermal comfort in residential building. *Desalination*, 209: 261–268.